

# Tables of Hyperonic Matter Equation of State for Core-Collapse Supernovae ‡

Chikako Ishizuka<sup>1</sup>, Akira Ohnishi<sup>1,2</sup>, Kohsuke Tsubakihara<sup>1</sup>  
Kohsuke Sumiyoshi<sup>3</sup> and Shoichi Yamada<sup>4</sup>

<sup>1</sup> Department of Physics, Faculty of Science,  
Hokkaido University, Sapporo 060-0810, Japan

<sup>2</sup> Yukawa Institute for Theoretical Physics, Kyoto University, Kyoto, Japan

<sup>3</sup> Numazu College of Technology, Numazu, Japan

<sup>4</sup> Science and Engineering, Waseda University, Tokyo, Japan

E-mail: [chikako@nucl.sci.hokudai.ac.jp](mailto:chikako@nucl.sci.hokudai.ac.jp), [ohnishi@yukawa.kyoto-u.ac.jp](mailto:ohnishi@yukawa.kyoto-u.ac.jp),  
[sumi@numazu-ct.ac.jp](mailto:sumi@numazu-ct.ac.jp)

**Abstract.** We present sets of equation of state (EOS) of nuclear matter including hyperons using an  $SU_f(3)$  extended relativistic mean field (RMF) model with a wide coverage of density, temperature, and charge fraction for numerical simulations of core collapse supernovae. Coupling constants of  $\Sigma$  and  $\Xi$  hyperons with the  $\sigma$  meson are determined to fit the hyperon potential depths in nuclear matter,  $U_\Sigma(\rho_0) \simeq +30\text{MeV}$  and  $U_\Xi(\rho_0) \simeq -15\text{MeV}$ , which are suggested from recent analyses of hyperon production reactions. At low densities, the EOS of uniform matter is connected with the EOS by Shen et al., in which formation of finite nuclei is included in the Thomas-Fermi approximation. In the present EOS, the maximum mass of neutron stars decreases from  $2.17M_\odot$  ( $Ne\mu$ ) to  $1.63M_\odot$  ( $NYe\mu$ ) when hyperons are included. In a spherical, adiabatic collapse of a  $15M_\odot$  star by the hydrodynamics without neutrino transfer, hyperon effects are found to be small, since the temperature and density do not reach the region of hyperon mixture, where the hyperon fraction is above 1 % ( $T > 40\text{MeV}$  or  $\rho_B > 0.4\text{ fm}^{-3}$ ).

## 1. Introduction

The equation of state (EOS) plays an important role in high density phenomena such as high energy heavy-ion collisions, neutron stars, supernova explosions, and black hole formations [1, 2, 3, 4, 5, 6, 7, 8, 9, 10, 11, 12, 13, 14]. The recent discovery of the strongly interacting quark gluon plasma (sQGP) [14] attracts attentions to the EOS and transport coefficients in the quark gluon plasma (QGP). The core region of neutron stars, where matter becomes very dense ( $\sim 10^{15}\text{g/cm}^3$ ), is an interesting play ground of quark and hadronic matter models. Various ideas for the new form inside neutron stars have been proposed including strangeness and quark degrees of freedom [1, 2, 3, 4, 5, 6, 7, 8, 9]. Core-collapse supernovae also involve high density

‡ <http://nucl.sci.hokudai.ac.jp/~chikako/EOS>

and temperature. The nuclear repulsion at high densities drives the shock wave at core bounce and the passage of shock wave heats up the matter inside the supernova core. A hot, lepton-rich neutron star (proto-neutron star) is born after the explosion and cools down by emitting supernova neutrinos. When black holes are formed for more massive cores, extremely high density and temperature are involved, where hyperons should appear and quarks would be deconfined. In order to describe the whole evolution of core-collapse supernovae by numerical simulations, one needs to prepare the set of microphysics under such extreme conditions. One of the most important ingredients is the set of equation of state (EOS) that contains necessary physical quantities. It is to be noted that one must cover a wide range of temperature, density and composition in a consistent manner and theoretical framework.

Until now, the two sets of EOS (Lattimer-Swesty EOS [15] and Shen EOS [16]) have been widely used and applied to numerical simulations of core-collapse supernovae [10, 11] and black hole formations [12, 13]. The Lattimer-Swesty EOS is based on a compressible liquid-drop model, whose mass and mean field potential are motivated by non-relativistic zero-range Skyrme type interactions. The Shen EOS is based on a relativistic mean field (RMF) model, whose interactions are determined by fitting the binding energies and nuclear radii of stable as well as unstable nuclei [17]. Coexistence of nuclei and uniform matter is included in the Thomas-Fermi approximation in the Wigner-Seitz cell, and the alpha particles are assumed to follow the statistical distribution with excluded volume effects.

The constituents in these EOSs are neutrons, protons, alpha-particles and nuclei, restricting the framework within the non-strange baryons. These degrees of freedom may be enough to simulate the early stage of hydrodynamical evolution of supernova explosions. However, in order to clarify the long-time evolution from core collapse [11] to proto-neutron star cooling [18, 19], black hole formation [12, 13], neutron star mergers and gamma ray bursts that may involve higher density/temperature, it would be necessary to include other particle degrees of freedom. Especially, hyperons (baryons containing strange quarks) are commonly believed to appear in neutron star core and to modify the neutron star profile [1, 2, 3, 4, 5, 6, 7]. While there are several works which include the hyperons in the proto-neutron star cooling [19], there has been no study on the dynamics of core-collapse supernovae adopting the EOS with hyperons. This is partially because EOS table of supernova matter including hyperons has not been available in public. In addition, the determination of the interaction for hyperons has been difficult having large uncertainties so far.

Recently, developments in hypernuclear physics have narrowed down the allowed range of hyperon potential depth in nuclear matter. The potential depth of  $\Lambda$  has been well known to be around  $U_{\Lambda}^{(N)}(\rho_0) \simeq -30\text{MeV}$  from bound state spectroscopy. For  $\Sigma$  baryons, it was considered to feel similar potential to  $\Lambda$ , because it contains the same number of light ( $u, d$ ) quarks. From the recently observed quasi-free  $\Sigma$  production spectra [20], it is now believed that  $\Sigma$  baryons would feel repulsive potential in nuclear matter;  $U_{\Sigma}(\rho_0) \simeq +30\text{MeV}$  [21, 22, 23]. Also for  $\Xi$  baryons, the analyses of

the twin hypernuclear formation [24] and the  $\Xi$  production spectra [25, 26, 27], suggest the potential depth of around  $U_{\Xi}^{(N)}(\rho_0) \simeq -15\text{MeV}$ . These  $\Sigma$  and  $\Xi$  hyperons are particularly important in neutron stars, since nuclear matter can take a large energy gain from neutron Fermi energy and symmetry energy by replacing, for example, two neutrons with a proton and a negatively charged hyperon ( $\Sigma^-$  or  $\Xi^-$ ). The updates on the interactions of hyperons may have impact on supernova dynamics and thermal evolution of proto-neutron stars.

In this paper, we present new sets of EOS of dense matter with hyperons, abbreviated as EOSY, under the current understanding of interaction. We provide the data table covering a wide range of temperature ( $T$ ), density ( $\rho_B$ ), and charge-to-baryon number ratio in hadronic part ( $Y_C$ ), which enables one to apply to supernova simulations. Our framework is based on the RMF theory with the parameter set TM1 [17], which was used to derive the EOS table by Shen et al. [16], and is extended to include hyperons by considering the flavor SU(3) Lagrangian [2]. Therefore, our EOS table is smoothly connected with Shen EOS and can be used easily as an extension of Shen EOS table in numerical simulations.

It is well known that the RMF predicts large values of incompressibility ( $K \sim 300$  MeV) and symmetry energy, and these are sometimes considered to cause problems in applying to dense matter EOS, since they lead to too high maximum mass of neutron stars without hyperons and may be unfavorable to core-collapse explosions. It should be noted that  $K$  and symmetry energy values are not yet well determined separately in a model independent manner. Analyses of collective flow data at AGS energies suggest  $K = 210 - 300$  MeV [28, 29], and collective flows at SPS energies are shown to be more sensitive to the mean field of resonance hadrons rather than to the cold matter EOS [30]. For symmetry energy, it is possible to describe binding energies, proton-neutron radius differences and isovector giant monopole resonances simultaneously by incorporating density dependent coupling (DD-ME1) in RMF and relativistic RPA [31] with a larger value of symmetry energy than that in non-relativistic models. Note that the interaction of RMF-TM1 is constrained by the nuclear masses, radii, neutron skins and excitations [17]. The large value of  $K$  leads to a large neutron star mass (stiff EOS), which seems not preferable for explosion. On the other hand, the large symmetry energy is known to be preferable for explosion, having less free proton fraction and smaller electron captures. These two effects are competing each other in the sophisticated numerical simulations [11]. We note also that the RMF fulfills automatically the causality (the sound velocity should not exceed the light velocity) whereas the non-relativistic frameworks breaks down at high densities appearing in the simulations. Thus at present we do not find problems in applying RMF EOS to dense matter compared to non-relativistic models.

This paper is arranged as follows. In section 2, we describe the framework to calculate the dense matter at finite temperature including hyperons. We explain the updated information on hyperon potentials in nuclear matter and adopted potential values in EOSY. We describe also the prescriptions to provide the data table for

the wide range of density including sub-saturation densities where finite nuclei appear. In section 3, we report the properties of EOSY in comparisons with nucleonic EOS (TM1/Shen EOS). We apply EOSY to cold neutron star matter and supernova matter. We show several properties of EOSY at finite temperatures by examining energies, chemical potentials and compositions. The data tables are successfully applied to hydrodynamical calculations of adiabatic collapse of iron core of massive stars. We examine the possibilities of hyperon appearance in supernova cores. Summary and discussions are given in section 4. In the appendix, we provide the definitions of quantities in EOSY.

## 2. Model and Method

In this work, we construct the EOS table of supernova matter based on a relativistic mean field model. We adopt the parameter set TM1 [17] for non-strange sector. For its flavor SU(3) extension, we start from the work by Schaffner and Mishustin [2], and we include the updated information on hyperon potentials from recent experimental and theoretical hypernuclear physics developments. Low density part of the EOS is connected with the Shen EOS.

### 2.1. Relativistic mean field model with hyperons

The relativistic mean field (RMF) theory is constructed to describe nuclear matter and nuclei based on the relativistic Brückner-Hartree-Fock theory [32], which successfully describes the nuclear matter saturation. It is preferable to adopt the relativistic frameworks for astrophysical applications, since they automatically satisfy the causality, *i.e.* the sound velocity is always less than the speed of light.

The RMF parameter set TM1 is determined to describe binding energies and nuclear radii of finite nuclei from Ca to Pb isotopes and fulfills the nuclear matter saturation. The incompressibility of symmetric uniform matter and the symmetry energy parameters are found to be  $K = 281$  MeV and  $a_{sym} = 36.9$  MeV. When it is applied to neutron stars, the maximum mass of cold neutron stars with TM1 is  $2.17M_{\odot}$ .

The extension of the RMF to flavor SU(3) has been investigated by many authors. A typical form of the Lagrangian density including hyperons is given as [2],

$$\begin{aligned} \mathcal{L} = & \sum_B \bar{\Psi}_B (i\not{\partial} - M_B) \Psi_B + \frac{1}{2} \partial^\mu \sigma \partial_\mu \sigma - U_\sigma(\sigma) \\ & - \frac{1}{4} \omega^{\mu\nu} \omega_{\mu\nu} + \frac{1}{2} m_\omega^2 \omega^\mu \omega_\mu - \frac{1}{4} \vec{R}^{\mu\nu} \cdot \vec{R}_{\mu\nu} + \frac{1}{2} m_\rho^2 \vec{R}^\mu \cdot \vec{R}_\mu \\ & - \sum_B \bar{\Psi}_B \left( g_{\sigma B} \sigma + g_{\omega B} \not{\omega} + g_{\rho B} \vec{\rho} \cdot \vec{t}_B \right) \Psi_B + \frac{1}{4} c_\omega (\omega^\mu \omega_\mu)^2 + \mathcal{L}^{YY} , \\ U_\sigma(\sigma) = & \frac{1}{2} m_\sigma^2 \sigma^2 + \frac{g_3}{3} \sigma^3 + \frac{g_4}{4} \sigma^4 , \end{aligned}$$

$$\begin{aligned} \mathcal{L}^{YY} = & \frac{1}{2} \partial_\nu \zeta \partial^\nu \zeta - \frac{1}{2} m_\zeta^2 \zeta^2 - \frac{1}{4} \phi_{\mu\nu} \phi^{\mu\nu} + \frac{1}{2} m_\phi^2 \phi_\mu \phi^\mu \\ & - \sum_B \bar{\Psi}_B (g_{\zeta B} \zeta + g_{\phi B} \gamma^\mu \phi_\mu) \Psi_B , \end{aligned} \quad (1)$$

where the sum runs over all the octet baryons. In this Lagrangian, hidden strangeness ( $\bar{s}s$ ) scalar and vector mesons,  $\zeta$  and  $\phi$ , are included in addition to  $\sigma$ ,  $\omega$  and  $\rho$  (represented by  $\vec{R}^\mu$ ) mesons. Strength tensors of  $\omega$ ,  $\rho$  and  $\phi$  mesons are shown in  $\omega^{\mu\nu}$ ,  $\vec{R}^{\mu\nu}$  and  $\phi^{\mu\nu}$ , respectively. The Lagrangian contains meson masses, coupling constants, and self-coupling constants as parameters.

In introducing hyperons in RMF, we have large ambiguities in hyperon-meson coupling constants. One of the ways to determine the parameters is to rely on symmetries. Schaffner and Mishustin [2] have determined hyperon-vector meson coupling constants based on the SU(6) (flavor-spin) symmetry,

$$\frac{1}{3} g_{\omega N} = \frac{1}{2} g_{\omega \Lambda} = \frac{1}{2} g_{\omega \Sigma} = g_{\omega \Xi}, \quad g_{\rho N} = \frac{1}{2} g_{\rho \Sigma} = g_{\rho \Xi}, \quad g_{\rho \Lambda} = 0, \quad (2)$$

$$2g_{\phi \Lambda} = 2g_{\phi \Sigma} = g_{\phi \Xi} = -\frac{2\sqrt{2}}{3} g_{\omega N}, \quad g_{\phi N} = 0. \quad (3)$$

Scalar mesons in RMF may partially represent contributions from some other components than  $\bar{q}q$ , such as  $\pi\pi$  in  $\sigma$ . In Ref. [2], the scalar meson couplings to hyperons have been given based on the assumption that hyperons feel potentials in nuclear and hyperon matter as,

$$\begin{aligned} U_\Lambda^{(N)} &= U_\Sigma^{(N)} = -30 \text{ MeV}, \quad U_\Xi^{(N)} = -28 \text{ MeV}, \\ U_\Sigma^{(\Sigma)} &\sim U_\Lambda^{(\Sigma)} \sim U_\Sigma^{(\Lambda)} \sim 2U_\Lambda^{(\Lambda)} \sim -40 \text{ MeV}, \end{aligned}$$

where  $U_B^{(B')}$  denotes the potential of  $B$  in baryonic matter at around  $\rho_0$  composed of  $B'$ . Recent developments in hypernuclear physics suggest that hyperon potentials in nuclear matter are repulsive for  $\Sigma$  [20, 21, 22, 23], and weakly attractive for  $\Xi$  [24, 25, 26, 27], respectively.

$\Xi$  hyperons are expected to have nuclear bound states, and the bound state spectroscopy at forthcoming facilities such as J-PARC and FAIR will give a strong constraints on the  $\Xi$  potential in nuclear matter. At present, the depth of the  $\Xi^-$ -nucleus potential has been suggested to be around 15 MeV from the analysis of twin hypernuclear formation [24] and the  $(K^-, K^+)$  spectrum in the bound state region [25]. In the former, the binding energy of the  $\Xi^-$ -nuclear system is found to be consistent with a shallow  $\Xi^-$ -nuclear potential in an event accompanied by two single hyperfragments emitted from a  $\Xi^-$  nuclear capture at rest (a twin hypernuclei) found in a nuclear emulsion [24]. In the latter, while the resolution of experimental data is not enough to distinguish the bound state peaks, the observed yield or the spectrum shape in the bound state region is found to be in agreement with the calculated results with  $U_\Xi^{(N)} \simeq -15 \text{ MeV}$  [25, 26, 27].

For  $\Sigma$  hyperons, it is necessary to analyze continuum spectra. In the observed (quasi-)bound  $\Sigma$  nucleus  ${}^4_\Sigma\text{He}$  [33], the coupling effect is strong and the repulsive contribution in the  $T = 3/2$ ,  ${}^3S_1$  channel is suppressed, then it does not strongly constrain the  $\Sigma$  potential in nuclear matter. The analysis of  $\Sigma^-$  atomic data suggested a

$\Sigma^-$ -nucleus potential having a shallow attractive pocket around the nuclear surface and repulsion inside the nucleus [34, 35, 36], but the atomic energy shift is not sensitive to the potential inside the nucleus. In the distorted wave impulse approximation (DWIA) analyses of the quasi free (QF) spectrum in the continuum region [20, 21, 22, 23], it is suggested that the  $\Sigma$  hyperon would feel repulsive real potential of  $10 \sim 90$  MeV. Recent theoretical analyses favor the strength of repulsion of around  $+30$  MeV [21, 22, 23]. This repulsion may come from the Pauli blocking effects between quarks due to the isovector nature of the diquark pair in  $\Sigma$  [37]. In a Quark-Meson Coupling (QMC) model, medium modification of the color hyperfine interaction in the quark bag is found to be the origin of repulsive  $\Sigma$  potential [38]. The  $\Sigma$  potential in nuclear matter at saturation density is predicted to be around  $+30$  MeV (repulsion) in a quark cluster model  $YN$  potential [37], and a chiral model also predicts a similar repulsion [39].

From these discussions, we adopt the following potential strength as *recommended* values,

$$U_{\Sigma}^{(N)}(\rho_0) \simeq +30 \text{ MeV}, \quad U_{\Xi}^{(N)}(\rho_0) \simeq -15 \text{ MeV}. \quad (4)$$

The above spectroscopic studies have been done mainly with non-relativistic frameworks for hyperons, then the potential should be regarded as the Schrödinger equivalent potential in RMF. The Schrödinger equivalent potential is related to the scalar ( $U_s$ ) and vector ( $U_v$ ) potentials as,

$$\begin{aligned} U_B(\rho, E(\mathbf{p})) &= U_s(\rho) + \frac{E(\mathbf{p})}{M_B} U_v(\rho) \\ &= g_{\sigma B} \sigma + g_{\zeta B} \zeta + \frac{E}{M} (g_{\omega B} \omega + g_{\rho B} R + g_{\phi B} \phi), \end{aligned} \quad (5)$$

where  $R$  represents the expectation value of the  $\rho$  meson. We have fixed  $g_{\sigma B}$  value by fitting the hyperon potential depth in normal symmetric nuclear matter,

$$U_B^{(N)}(\rho_0) = g_{\sigma B} \sigma^{(N)}(\rho_0) + g_{\omega B} \omega^{(N)}(\rho_0), \quad (6)$$

where  $\sigma^{(N)}(\rho_0)$  and  $\omega^{(N)}(\rho_0)$  represent the expectation values of  $\sigma$  and  $\omega$  mesons in symmetric nuclear matter at  $\rho_0$ . We adopt the parameter set TM1 for nucleon sector, and we determine  $g_{\sigma \Sigma}$  and  $g_{\sigma \Xi}$  to reproduce the potential depths of  $\Sigma$  and  $\Xi$  hyperons in Eq. (4) as listed in Table 1. We choose other hyperon-meson coupling constants referring to the values in Ref. [2]. We show the values of  $g_{\sigma \Sigma}$  and  $g_{\sigma \Xi}$  for different potentials in Table 2.

In the literature, the instability due to the negative effective mass of nucleon has been reported [40, 41]. As  $\sigma$  increases, the nucleon effective mass reaches zero at  $\sigma = M_N/g_{\sigma N}$  where hyperon effective masses are still positive and act to further increase  $\sigma$ , leading to the nucleon negative effective mass. This effect depends very much on  $\sigma Y$  couplings, which are small within the current sets of parameters, and we did not find this instability in the range of data tables. However, we found this instability occurs at very high densities/temperatures which are relevant in the black hole formation [42].



**Table 1.** The coupling constants of the parameter sets.

	$m_\sigma$ (MeV)	$g_3$ (MeV)	$g_4$	$c_\omega$
	511.198	1426.466	0.6183	71.3075

$g_{MB}$	$\sigma$	$\zeta$	$\omega$	$\rho$	$\phi$
$N$	10.0289	0	12.6139	4.6322	0
$\Lambda$	6.21	6.67	8.41	0	-5.95
$\Sigma$	4.36	6.67	8.41	9.26	-5.95
$\Xi$	3.11	12.35	4.20	4.63	-11.89

**Table 2.** The coupling constants of  $\Sigma N$  and  $\Xi N$ .

$U_\Sigma^{(N)}(\rho_0)$ (MeV)	$g_{\sigma\Sigma}$
+90	2.58
+30	4.36 present
0	5.35
-10	5.63
-30	6.21 Ref. [2]

$U_\Xi^{(N)}(\rho_0)$ (MeV)	$g_{\sigma\Xi}$
-15	3.11 present
-28	3.49 Ref. [2]

## 2.2. Free thermal pions

In black hole formation processes as found in Ref. [12], the temperature goes up to around 100 MeV. At these high temperatures, pion contributions become dominant. Charged pions may condensate at high densities in neutron star matter [1, 8]. To estimate the effect of pion mixtures, we also prepare the EOS table including free thermal pions assuming the pion mass is not affected by the interaction. This is of course oversimplification, however, the first trial to include pions. Further sophisticated studies are necessary.

The density of free thermal pions is calculated to be

$$\rho_\pi = \rho_\pi^{Cond} + \int \frac{d^3p}{(2\pi)^3} \frac{1}{\exp((E_\pi(\mathbf{p}) - \mu_\pi)/T) - 1}, \quad (7)$$

where  $\mu_\pi = \mu_C, 0, -\mu_C$  for  $\pi^+, \pi^0, \pi^-$ , respectively. When the absolute value of the chemical potential reaches the pion mass, pion condensation occurs; *i.e.* the amount of condensed  $\pi$  at zero momentum can take any value at  $\mu_C = \pm m_\pi$ . We have determined the amount of condensed  $\pi$  in the following way. First we solve the equilibrium condition and obtain  $\mu_B$  and  $\mu_C$  without condensed  $\pi$ . When  $|\mu_C| > m_\pi$ , we set  $|\mu_C| = m_\pi$  and re-evaluate hadron densities except for the condensed  $\pi$  to satisfy the condition of

$\rho_B = \rho_B(\text{Given})$ . Finally, the amount of condensed  $\pi$  is given so as to satisfy the charge density condition,  $\rho_C = Y_C(\text{Given})\rho_B$ .

The pion condensation in the current treatment is a simple  $s$ -wave Bose-Einstein condensation, which is different from the pion condensation derived from  $p$ -wave  $\pi N$  interaction [8]. We mention that pion condensation will be suppressed after considering  $s$ -wave  $\pi N$  repulsive interaction discussed in the energy shift of deeply bound pionic atoms [43, 44, 45] and in pion-nucleus scattering [46].

### 2.3. Low density

By using these potentials, we can immediately obtain a EOS of uniform dense matter with strangeness based on the RMF theory. We also need to cover the low-density region below  $\rho_0$ , where the inhomogeneous matter appears. Here we connect the uniform matter EOS with Shen EOS [16], which is based on the same RMF parameter set TM1 and treats the inhomogeneity with the Thomas-Fermi approach.

We include the contribution from inhomogeneity by adding the free energy difference of Shen EOS values from those in uniform matter,

$$F = F_{RMF}^Y + \Delta F_{Nucl} \quad (8)$$

at  $\rho_B \leq \rho_0$ , where

$$\Delta F_{Nucl} = F_{Shen} - F_{RMF}^{(np)} . \quad (9)$$

Other variables are derived in the same way as the above equations. The deviation due to inhomogeneity  $\Delta F$  vanishes at  $\rho_B > \rho_0$ . These prescriptions produce the extended EOS tables for studies in astrophysics, containing inhomogeneity at low density and strangeness information. The compositions of  $n, p, \alpha, A, Y$  are consistent with Shen EOS table and the sum of each component ratio becomes unity.

### 2.4. Tabulation of thermodynamical quantities

Thermodynamical quantities are provided in the data table as a function of baryon mass density  $\rho_B$ , charge ratio  $Y_C$ , and temperature  $T$ . Here  $Y_C$  means the charge ratio defined as  $Y_C = n_C/n_B$  and  $n_C$  is a charge density. See Appendix for the list of quantities and their definitions, which are slightly revised from the original table of Shen EOS.

For the purpose of numerical simulations, we prepare the EOS table containing the contributions of leptons and photons by adding the energy, pressure and entropy from electrons, positrons and photons to the hadronic EOS. We treat electrons and positrons as ideal Fermi gas with the finite rest mass and calculate photons according to the standard expressions for radiations.

The baryon mass density, charge ratio and temperature cover the following range,

- $\rho_B = 10^{5.1} \sim 10^{15.4} \text{ (g/cm}^3\text{)}$  (104 points)
- $Y_C = 0 \text{ and } 0.01 \sim 0.56$  (72 points)
- $T = 0 \text{ and } 0.1 \sim 100 \text{ (MeV)}$  (32 points)



Mesh points for  $\rho_B$ ,  $Y_C(>0)$  and  $T(>0)$  are taken as approximate geometric sequences with  $\Delta \log_{10} \rho_B = 0.1$ ,  $\Delta \log_{10} Y_C = 0.025$  ( $-2.00 \leq \log_{10} Y_C \leq -0.25$ ) and  $\Delta \log_{10} T \simeq 0.1$ , respectively. These ranges and mesh points are the same as those in Shen EOS. By connecting smoothly in the way described above, the EOS table is combined with Shen EOS at lower densities below  $\rho_0$  while it includes full baryon octet at high densities so that one can see the effects of hyperon mixture. Some tabulated quantities in the EOS table need attentions. The values of the mass  $A$  and charge number  $Z$  of heavy nucleus are taken from Shen EOS at densities below  $\rho_0$  and are set to be zero above  $\rho_0$ . Similarly, the fraction of  $\alpha$ -particle and heavy nucleus are taken from Shen EOS at low densities and are set to be zero at high densities.

### 3. Properties of EOS tables and astrophysical applications

We report the properties of dense matter in the present EOS table with hyperons (EOSY) and their applications to neutron stars and supernovae. We adopt hereafter the case of  $(U_\Sigma^{(N)}(\rho_0), U_\Xi^{(N)}(\rho_0)) = (+30 \text{ MeV}, -15 \text{ MeV})$  as a standard case, which is currently the most recommended set of hyperon potentials. We also consider the case with pion contribution (EOSY $\pi$ ) and the attractive hyperon potential case [2]  $(U_\Sigma^{(N)}(\rho_0), U_\Xi^{(N)}(\rho_0)) = (-30 \text{ MeV}, -28 \text{ MeV})$ , abbreviated as EOSY(SM).

#### 3.1. Neutron star matter

We first study the EOS of neutron star matter, which is under the  $\beta$  equilibrium at zero temperature. We here add electron and muon contributions under the  $\beta$  equilibrium and charge neutrality conditions. We consider uniform matter ignoring finite nuclear effects.

We show particle compositions in neutron star matter in Fig. 1 to see the appearance of new degrees of freedom. We display the cases of nucleonic (TM1, upper-left) and hyperonic (EOSY, upper-right) EOS. Results with hyperonic EOS with attractive  $\Sigma$  potential (EOSY(SM), lower-left) and hyperonic EOS with pions (EOSY $\pi$ , lower-right) are also shown for comparison. The particle composition of neutron star matter is very sensitive to the choice of hyperon potentials. With attractive  $\Sigma$  potential,  $\Sigma^-$  appears at lower densities than  $\Lambda$ . With repulsive  $\Sigma$  potential,  $\Lambda$  appears first followed by  $\Xi^-$  and  $\Xi^0$ . This behavior is different from the previous works that adopt attractive potentials [1, 2, 3, 4, 5], and pointed out in Refs. [2, 3, 4, 38]. When we allow the appearance of pions, condensed pions ( $\pi^-$ ) appear prior to hyperons. With  $\pi^c$  condensation, the charge chemical potential is restricted to be  $|\mu^c| \leq m_\pi$  and the proton fraction becomes larger, then the neutron chemical potential is reduced. As a result, the threshold density of hyperons are shifted up. The density of  $\Lambda$  appearance is about  $0.37 \text{ fm}^{-3}$  and other hyperons such as  $\Xi^-$  are also suppressed.

In the left panel of Fig. 2, we show the energy per baryon ( $E/B$ ) and chemical potentials ( $\mu_n$  and  $\mu_p$ ) in neutron star matter in nucleonic EOS (TM1), EOSY and

**Table 3.** Constituents, assumed hyperon potentials, threshold densities, maximum masses of neutron stars, central densities giving maximum masses of neutron stars and neutron star masses at the threshold central densities in nucleonic EOS (TM1/Shen EOS [17, 16]), hyperonic EOS with attractive hyperon potentials (EOSY(SM) [2]), hyperonic EOS with repulsive hyperon potentials (EOSY, present work) and hyperonic EOS with repulsive hyperon potentials including pions (EOSY $\pi$ , present work). For  $\pi^-$ , the maximum density of condensation is also shown in parentheses. Threshold densities of protons and muons are  $1.1 \times 10^{-4} \text{ fm}^{-3}$  and  $0.11 \text{ fm}^{-3}$ , respectively.

EOS	TM1/Shen EOS	EOSY(SM)	EOSY	EOSY $\pi$
Constituents	$Ne(\mu)$	$NYe(\mu)$	$NYe(\mu)$	$NY\pi e(\mu)$
$U_{\Sigma}^{(N)}$ (MeV)		-30	+30	+30
$U_{\Xi}^{(N)}$ (MeV)		-28	-15	-15
$\rho_{(thr)}$ (fm $^{-3}$ )				
$\Lambda$		0.32	0.32	0.37
$\Sigma^-$		0.29	1.14	1.1
$\Sigma^0$		0.57	1.34	1.3
$\Sigma^+$		0.69	1.47	1.5
$\Xi^-$		0.43	0.40	0.56
$\Xi^0$		0.62	0.71	0.74
$\pi^-$				0.16(0.88)
$M_{NS}^{(max)}$ ( $M_{\odot}$ )	2.17	1.55	1.63	1.65
$\rho_B^{(max)}$ (fm $^{-3}$ )	1.12	0.79	0.79	0.97
$M_{NS}^{(thr)}$ ( $M_{\odot}$ )		1.17( $\Sigma^-$ )	1.28( $\Lambda$ )	1.22( $\Lambda$ ) 0.51( $\pi^-$ )

EOSY $\pi$ . Compared with nucleonic EOS,  $E/B$  is much lower in EOSY at high densities. Chemical potentials are also suppressed with hyperons correspondingly. There are several origins for this energy gain. First, nucleon Fermi energy decreases due to the hyperon mixture. Secondly, the lepton contribution is suppressed when negatively charged hyperons emerge. In addition, the repulsive vector potential becomes small, because the  $\omega Y$  couplings are smaller than  $\omega N$  and the isospin asymmetry becomes smaller when negatively charged hyperons appear, as shown in the long-dashed lines in Fig. 3.

For  $E/B$  and  $\mu_n$ , pionic effects are small and only visible around  $\rho_B \sim 0.4 \text{ fm}^{-3}$ , while we find large differences in  $\mu_p$ . The equality  $\mu_C = \mu_p - \mu_n = -m_{\pi}$  under  $\pi^-$  condensation reads the Fermi energy relation,  $E_F(n) = E_F(p) + m_{\pi}$ . Since a neutron on the Fermi surface is replaced with a proton and a  $\pi^-$  having the same total energy, we have to pay the cost of the pion rest mass energy in exchange for the Fermi energy reduction and symmetry energy gain. At higher densities where hyperons appear, pionic effects becomes smaller, and disappear at  $\rho_B = 0.88 \text{ fm}^{-3}$ .

The  $s$ -wave pion condensation would be suppressed when we include the  $\pi N$

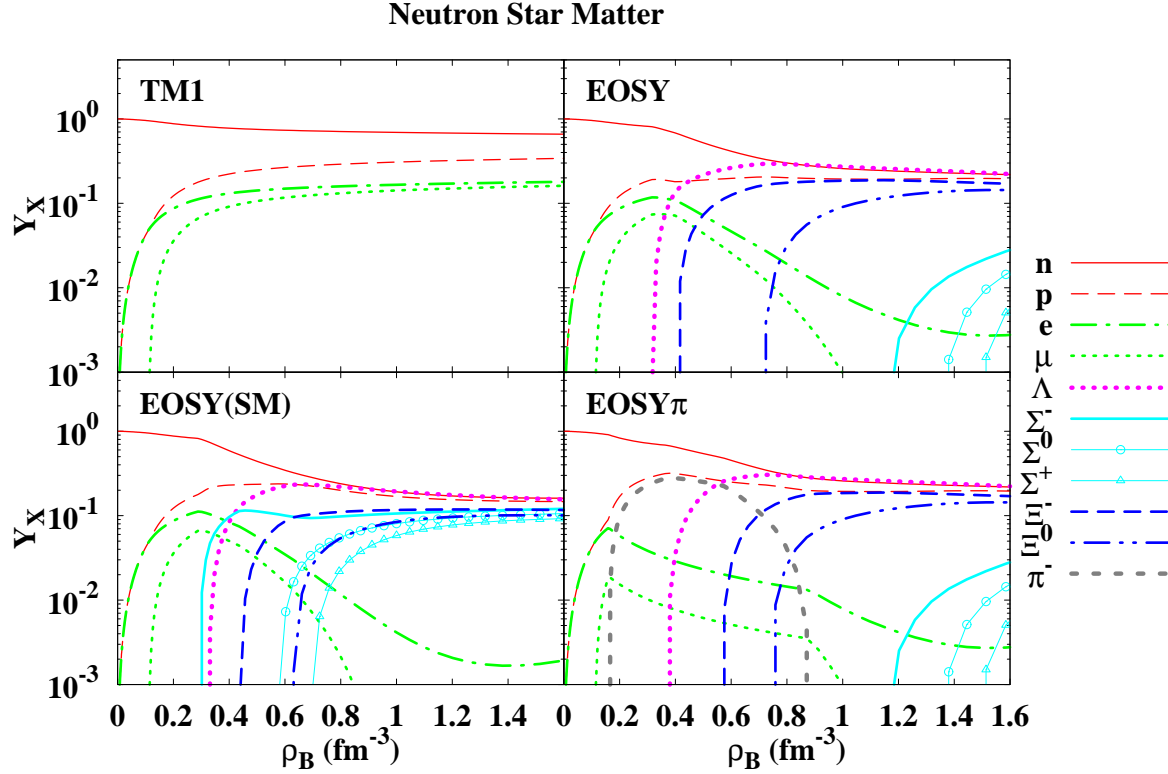


**Figure 1.** Composition of neutron star matter in nucleonic EOS (TM1, upper-left), hyperonic EOS with attractive potential (EOSY(SM), lower-left), hyperonic EOS with repulsive potential without (EOSY, upper-right) and with pions (EOSY $\pi$ , lower-right). The number fraction of particles are plotted as functions of baryon density. The species of particles are denoted as in the legend.

interaction. We evaluate the pion energy by using the potential of the form [43, 44, 45, 46],

$$U_s(\pi^-) = -\frac{2\pi}{m_\pi} \left[ \left(1 + \frac{m_\pi}{M_N}\right) (b_0 \rho_B + b_1 \delta\rho) + \left(1 + \frac{m_\pi}{2M_N}\right) \text{Re}B_0 \rho_B^2 \right], \quad (10)$$

where  $b_1 = b_1^{\text{free}}/(1 - \alpha\rho_B/\rho_0)$ ,  $\delta\rho = \rho_n - \rho_p$ . As typical examples, we adopt the parameter sets from the analyses of pionic atom data;  $b_0 = -0.023/m_\pi$ ,  $b_1 = -0.085/m_\pi$  ( $\alpha = 0$ ),  $\text{Re}B_0 = -0.021/m_\pi^4$  (less repulsive) [44], and  $b_0 = -0.0233/m_\pi$ ,  $b_1^{\text{free}} = -0.1473/m_\pi$ ,  $\alpha = 0.367$  ( $b_1 = -0.1149/m_\pi$  at  $\rho_B = 0.6\rho_0$ ),  $\text{Re}B_0 = -0.019/m_\pi^4$  (more repulsive) [45]. In Fig. 3, we show the pion energy,  $E_\pi = \sqrt{m_\pi^2 + 2m_\pi U_s}$ , calculated with these potentials and proton fraction in TM1 EOS. With these potentials, we find that the existence of the  $s$ -wave pion condensed region,  $E_\pi < \mu_e$ , depends on the pion optical potential parameters. Since the pion potential above the normal nuclear density is not yet known, the realization of pion condensation may be marginal and model-dependent.

We apply the above four EOSs of neutron star matter discussed above (TM1 EOS, EOSY(SM), EOSY, EOSY $\pi$ ) to the hydrostatic structure of neutron stars by solving the Tolman-Oppenheimer-Volkoff equation. We plot the gravitational mass of neutron

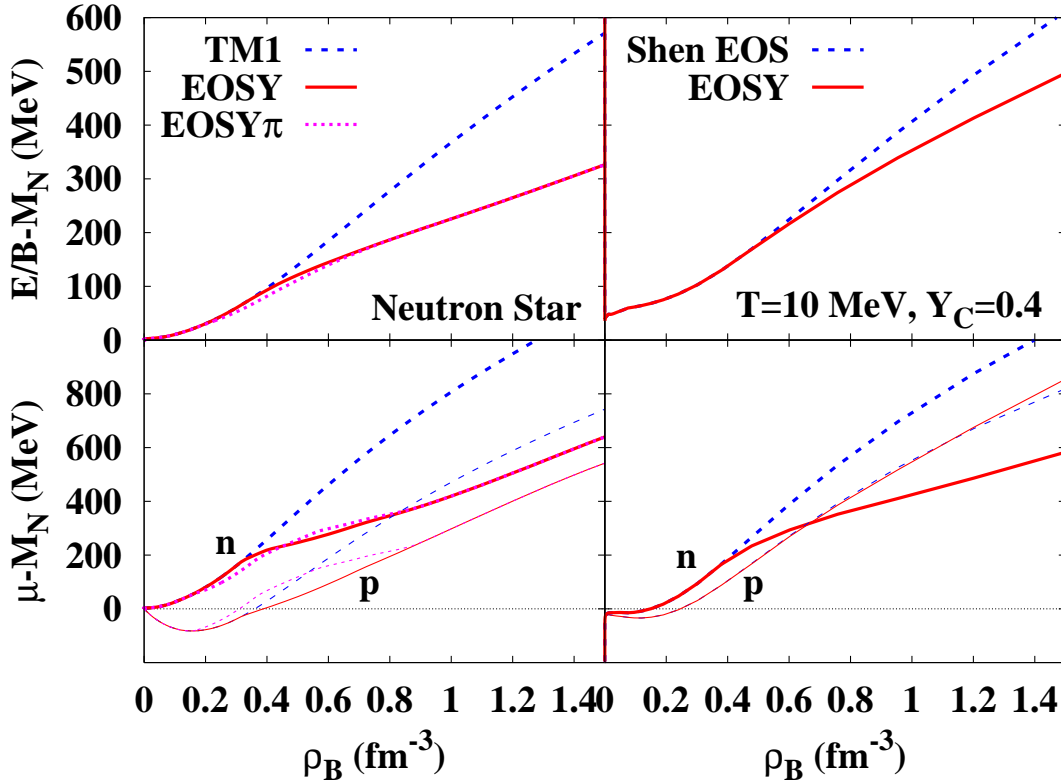


**Figure 2.** EOS of neutron star matter and supernova matter for nucleonic EOS (TM1/Shen EOS), hyperon EOS(EOSY), hyperon EOS with free pions (EOSY $\pi$ ). The upper panels display the energy per baryon, and the lower panels the chemical potentials of proton and neutron. The dashed line is for the nucleonic EOS, the solid line is for hyperon EOS (EOSY), and dotted line is for hyperon EOS with pions (EOSY $\pi$ ).

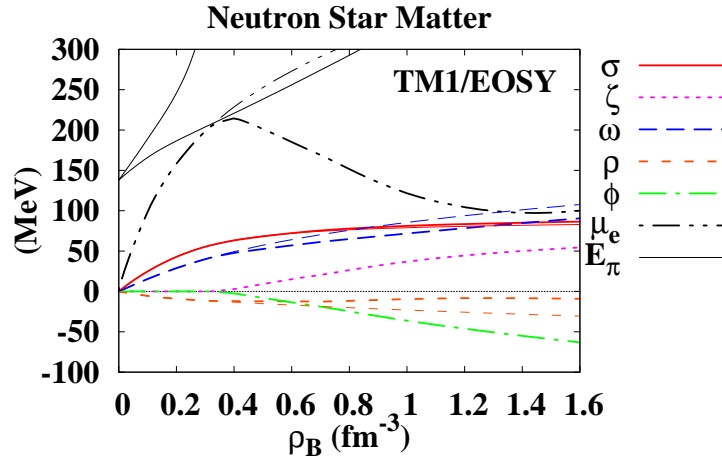


**Figure 3.** Meson expectation values and electron chemical potential in neutron star matter for TM1 EOS (thin lines) and hyperon EOS(EOSY) (thick lines). Thin solid lines show the pion energy,  $E_\pi = \sqrt{m_\pi^2 + 2m_\pi U_s(\pi^-)}$ , where lower less repulsive (upper more repulsive) line shows the results with the pion optical potential in Ref. [44] ([45]) by using the proton fraction in TM1 EOS.

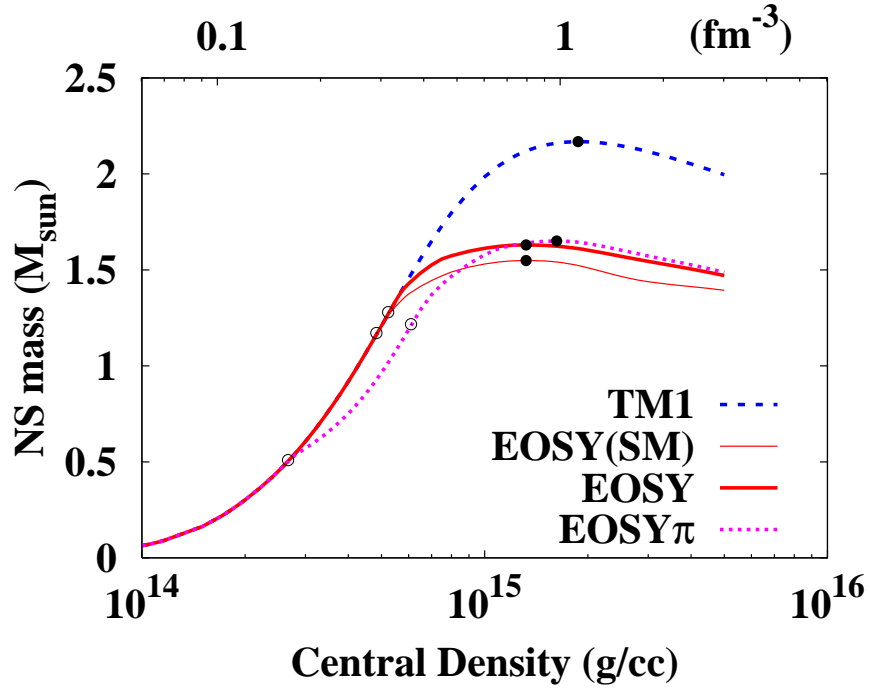


**Figure 4.** Neutron star masses are shown as functions of central density. The dashed, thin solid, thick solid, dotted lines show the results with nucleonic EOS (TM1 [17]), hyperonic EOS with attractive hyperon potentials (EOSY(SM) [2]), hyperonic EOS with repulsive hyperon potentials (EOSY) and hyperonic EOS with pions (EOSY $\pi$ ), respectively. Filled points show the maximum neutron star masses, and open circles show the threshold densities of hyperons and pions.

stars as a function of central baryon mass density in Fig.4. The maximum mass of neutron stars in EOSY is smaller than the case of nucleonic EOS because of the softness from hyperons. The maximum mass is  $1.63 M_{\odot}$  for EOSY in contrast to  $2.17 M_{\odot}$  for nucleonic EOS when we adopt repulsive potentials for hyperons. The maximum mass is further reduced to be  $1.55 M_{\odot}$  in EOSY(SM) with attractive potentials. The neutron star masses with EOSY $\pi$  are reduced in the mid range of central density  $0.16 \text{ fm}^{-3} < \rho_B < 0.8 \text{ fm}^{-3}$ , but the maximum mass ( $1.65 M_{\odot}$ ) is almost the same. This is because the maximum mass is mainly determined by the EOS at densities around  $0.8 \text{ fm}^{-3}$  or more, where the condensed pion density is small. The central density of a typical neutron star having  $1.4 M_{\odot}$  is  $0.35 \text{ fm}^{-3}$  in nucleonic EOS (TM1), which is a little above the threshold density of  $\Lambda$  in EOSY. In this case, hyperons are limited only in the core region, and the neutron star mass does not get a large reduction as seen in Fig. 4. We summarize the neutron star masses and the threshold densities to have hyperons in neutron star matter in Table 3.

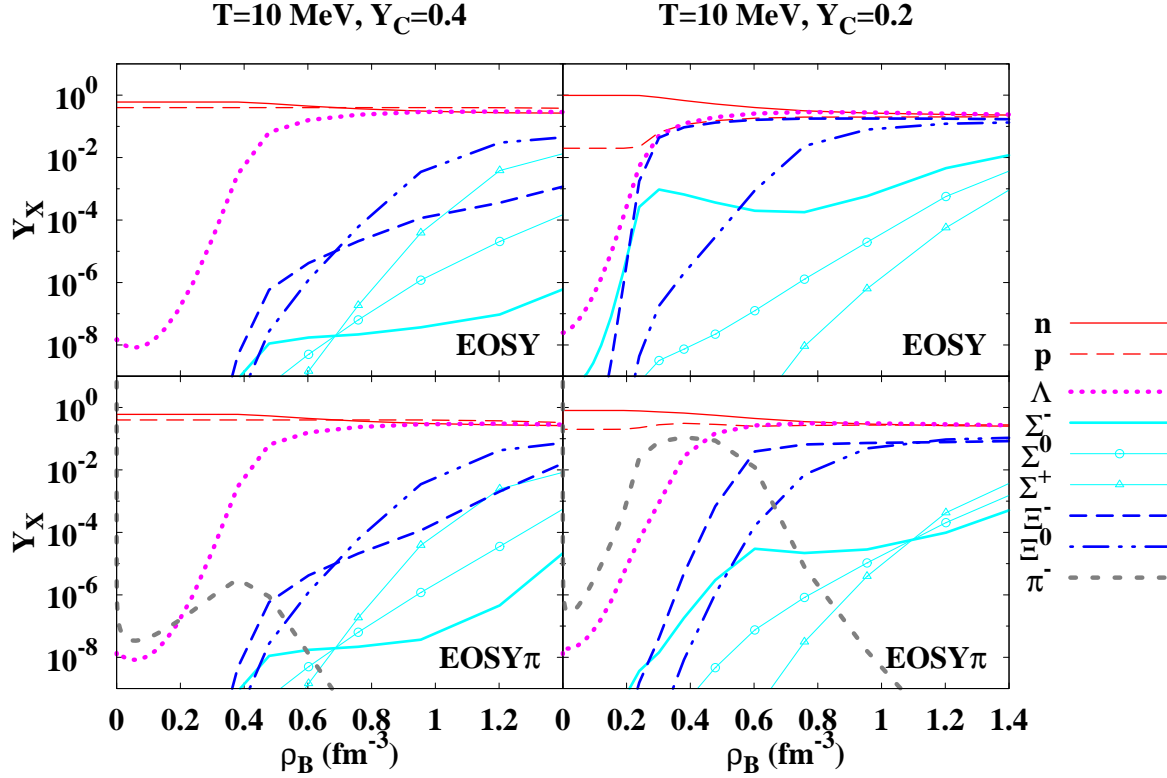


**Figure 5.** Composition of supernova matter at  $(T, Y_C) = (10 \text{ MeV}, 0.4)$  (left) and  $(T, Y_C) = (10 \text{ MeV}, 0.2)$  (right) in the hyperonic EOS table without (EOSY, upper) and with (EOSY $\pi$ , lower) pions. The number fraction of particles are plotted as functions of baryon density. The species of particles are denoted as in the legend.

### 3.2. Hyperonic matter at finite temperatures

We next study the EOS of supernova matter, where the hadronic charge fraction ( $Y_C$ ) is fixed at finite temperature. We here show the results including electron and photon contributions. Finite nuclear effects in Shen EOS are included. The treatment of leptons in supernova matter are explained in Appendix A.4.

In order to demonstrate the contents of the EOS table, we show the energy and compositions as functions of baryon density by choosing  $T = 10 \text{ MeV}$  and  $Y_C = 0.4$  as an example. In the upper-right panel of Fig. 2, we plot energy per baryon ( $E/B$ ) in EOSY together with the results in Shen EOS for comparison. At  $\rho_B > 0.4 \text{ fm}^{-3}$ , the energy is lower in EOSY than in Shen EOS due to hyperons (See Fig. 5). In the lower-right panel of Fig. 2, neutron and proton chemical potentials are shown. In EOSY, the difference of chemical potentials between neutron and proton is small and neutron chemical potential becomes smaller than proton chemical potential at  $0.7 \text{ fm}^{-3}$ . This is because more  $SU_f(3)$  symmetric matter is preferred toward high densities, and the charge fraction under  $\beta$  equilibrium decreases below  $Y_C = 0.4$  at high densities.

We show the particle compositions as functions of baryon density in EOSY and EOSY $\pi$  at  $Y_C = 0.4$  in the left panels of Fig. 5. In moderately isospin asymmetric



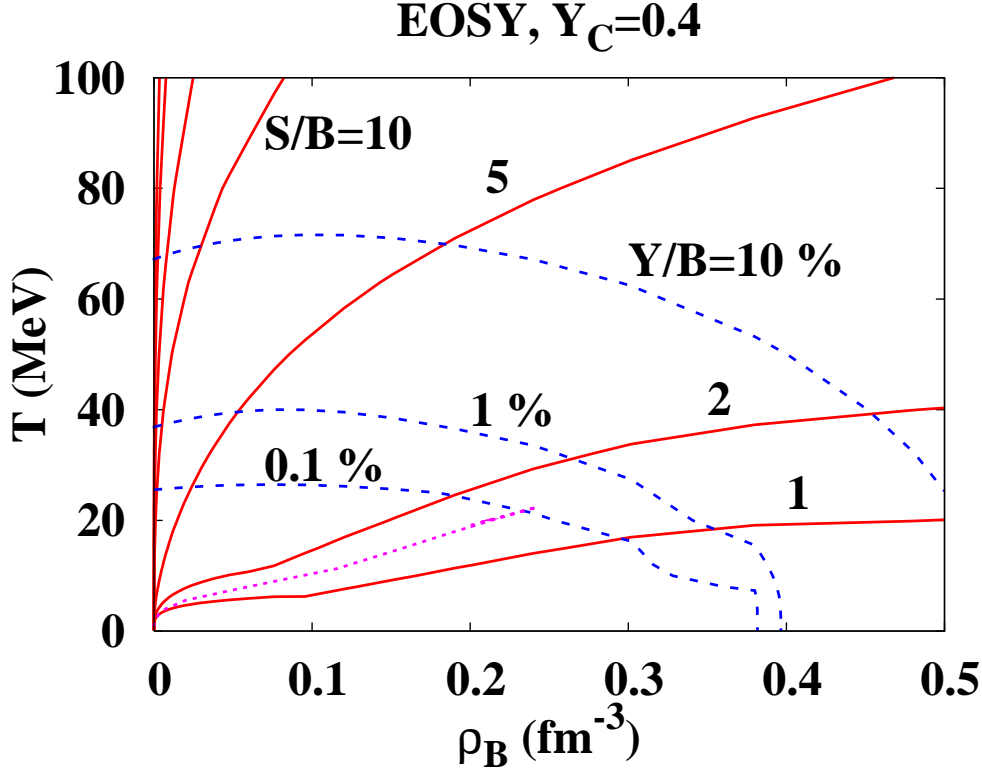


**Figure 6.** Hyperon fraction contours and adiabatic paths in supernova matter at  $Y_C = 0.4$  from the hyperonic EOS table without pions (EOSY). The contours of the fixed number fraction of hyperons (sum of strange baryons) are shown by dashed lines. The solid lines denote the contour of fixed entropy per baryon (isentropy). The dotted line shows the trajectory of the dense matter at center during core collapse and bounce.

matter ( $Y_C = 0.4$ ), the fraction of  $\Lambda$  particle grows at around  $\rho_B \sim 0.4 \text{ fm}^{-3}$ , and becomes comparable to nucleons at higher densities. The fractions of other strange baryons increase slowly and remains small until very high density. In the right panels of Fig. 5, we show the particle compositions at  $Y_C = 0.2$ . With this small charge fraction, total hyperon fraction reaches 1 % at  $0.25 \text{ fm}^{-3}$ .

In Fig. 6, we plot the contour map of the fraction of hyperons (sum of strange baryons) in the density-temperature plane. In order to have a significant amount of hyperons, one needs high density or temperature. In supernova core, the entropy per baryon is typically around 1–2  $k_B$ , therefore, one needs high densities  $0.3\text{--}0.4 \text{ fm}^{-3}$  to have 1% mixture of hyperons and  $0.45 \text{ fm}^{-3}$  for 10%.

In supernova matter, the effects of hyperons and pions are limited. When isospin asymmetry is not high (ex.  $Y_C = Y_e = 0.4$ ), total amount of hyperons which appears at  $0.4 \text{ fm}^{-3}$  is around 1% of baryons. The value of  $Y_C$  remains high due to the neutrino trapping during the collapse and bounce [48]. However, after the deleptonization due to neutrino emission,  $Y_C$  becomes smaller and hyperons may appear in the proto-neutron star cooling process. Dense matter at higher densities and temperatures may appear also in black hole formations, and hyperon effects can be expected in such processes.

### 3.3. Applications to core-collapse supernovae

As an application of the EOS table with hyperons, we perform the numerical calculations of hydrodynamics of core-collapse supernovae. This calculation is aimed to test the data of EOS table for numerical simulations and to provide the basic information on the properties of EOS in supernovae such as the appearance of hyperons. For this purpose, we calculate the adiabatic collapse of iron core of massive stars of  $15M_{\odot}$  [47]. In the same way as the hydrodynamical calculations in Sumiyoshi et al. [10], we calculate the general relativistic hydrodynamics under the spherical symmetry without neutrino-transfer, which is time-consuming, by assuming that the electron fraction is fixed to the initial value in the stellar model. Numerical simulations by neutrino-radiation hydrodynamics are in progress.

We have found that the adiabatic collapse of  $15M_{\odot}$  star with EOSY leads to a prompt explosion. This *model* explosion is caused by the large electron fraction assumed and is quite similar to the case obtained with Shen EOS [10]. The explosion energy is almost the same as the case with Shen EOS and the difference turns out to be small within 0.5%. We plot the trajectory of density and temperature of the central grid in the hydrodynamical calculation in Fig. 6.

We have examined the appearance of hyperons during the evolution of core-collapse and bounce. We find that the fraction of hyperons turn out to be very small within  $10^{-3}$ . This is because the density does not increase drastically even at the core bounce in the current model. The peak density is  $0.24 \text{ fm}^{-3}$  which is lower than the threshold density  $0.60 \text{ fm}^{-3}$  at temperature 21.5 MeV and electron fraction 0.42, where  $\Lambda$  hyperons appear by the same order as nucleons. This small mixture does not affect largely the dynamics in the model explosion.

A large electron fraction leads to a large proton fraction, and, therefore, suppresses the appearance of hyperons [48]. We note here that this is the outcome of simple adiabatic hydrodynamics without the treatment of neutrinos. When electron captures and neutrino trapping are taken into account [11], electron fraction might be smaller than the current value and may enhance the hyperon appearance. The hyperons will definitely appear in the thermal evolution of proto-neutron stars after 20 seconds [19], during which the central density becomes high and the electron fraction gets smaller. In recent findings of black hole formation from massive stars of  $40M_{\odot}$  [12, 13], the hyperon EOS is necessary since the density becomes extremely high during the collapse toward the black hole. It would be interesting to perform the full simulations of core-collapse supernovae and related astrophysical phenomena.

## 4. Summary and discussion

In this paper, we have presented several sets of equation of state (EOS) of supernova matter (finite temperature nuclear matter with lepton mixture) including hyperons (EOSY) using an  $SU_f(3)$  extended relativistic mean field (RMF) model with a wide

coverage of density, temperature, and charge fraction. Supernova matter EOS is one of the most essential parts in numerical simulations of core collapse supernovae. At present, two sets of supernova matter EOS (Lattimer-Swesty EOS [15] and Shen EOS [16]) are widely used. The constituents in these EOSs are nucleons and nuclei, then it is desired to include hyperons, which are believed to appear at high densities. Here we have extended the relativistic EOS by Shen et al. [16] by introducing hyperons.

We start from the RMF parameter set TM1 for nucleon sector [17], which well describes the bulk properties of nuclei in the wide mass and isospin range. For hyperon-meson coupling constants, we adopt the values in Ref. [2] as the starting points. Hyperon-vector meson couplings are fixed based on the flavor-spin SU(6) symmetry, and hyperon-scalar meson couplings are determined to give the hyperon potentials in nucleonic and hyperonic matter. Hyperon potentials in nuclear matter around the normal density,  $U_Y^{(N)}(\rho_0)$ , are accessible in hypernuclear production reactions. Recent developments in hypernuclear physics suggest the following potentials for  $\Sigma$  [21, 22, 23] and  $\Xi$  baryons [24, 25, 26, 27]

$$U_{\Sigma}^{(N)}(\rho_0) \simeq +30 \text{ MeV} , \quad U_{\Xi}^{(N)}(\rho_0) \simeq -15 \text{ MeV} . \quad (11)$$

These potentials are consistent with those in the quark-cluster model for  $YN$  interaction [37] and a chiral model prediction [39]. In this paper, we have modified  $g_{\sigma\Sigma}$  and  $g_{\sigma\Xi}$  to explain these potentials, while other coupling constants are unchanged from those in Ref. [2].

The  $\Sigma$  potential in nuclear matter still has ambiguities. Recent theoretical analysis [23] has shown that the shape and absolute values of quasi-free  $\Sigma$  production spectra are well explained in a Woods-Saxon potential with  $U_{\Sigma}(\rho_0) \simeq +15 \text{ MeV}$ . On the other hand, a few MeV attractive pocket is known to be required to explain the energy shift of  $\Sigma^-$  atom [34, 35, 36], then the central repulsion would be stronger to cancel the effects of this pocket. Other theoretical analyses [21, 22] suggest that  $U_{\Sigma}(\rho_0) \simeq +30 \text{ MeV}$  would be preferred in order to explain the shape or the absolute yield in  $\Sigma$  production spectra. In any of these analyses,  $\Sigma$  potential should be repulsive or less attractive than that for  $\Lambda$ , then the effects of  $\Sigma$  hyperons are much smaller than those in the attractive case. It is to be noted that the ambiguities in  $U_{\Sigma}$  do not affect the supernova EOS very much as far as  $\Sigma$  hyperon fraction is small.

Formation of finite nuclei at low densities is another important ingredient in supernova simulations. In the present EOS, effects of finite nuclear formation are included by using the Shen EOS [16], in which formation of finite nuclei is included in the Thomas-Fermi approximation. Effects from finite nuclei are evaluated by the difference of free energy and its derivatives in the Shen EOS from the EOS of uniform nucleonic matter (TM1) without hyperons at each  $(T, \rho_B, Y_C)$ .

We have examined the properties of the EOS with hyperons in neutron star matter ( $T = 0$ ,  $\beta$ -equilibrium) and supernova matter. Hyperon effects are significant in neutron stars as discussed already in the literature [1, 2, 3, 4, 5, 6, 7]. Hyperons appear at around  $\rho_B \simeq 2\rho_0$  in cold matter under  $\beta$ -equilibrium and soften the EOS. The maximum mass

of neutron stars decreases from  $2.17M_\odot$  to  $1.55M_\odot$  and  $1.63M_\odot$  when hyperons are included with attractive and repulsive hyperon potentials, respectively. In prompt phase in supernova explosions, on the other hand, hyperon effects are found to be small in a spherical, adiabatic collapse of a  $15M_\odot$  star by the hydrodynamics without neutrino transfer. In the case with  $Y_C = Y_e = 0.4$  as a typical example, hyperon fraction becomes meaningful ( $Y_Y > 1\%$ ) at  $\rho_B > 0.4 \text{ fm}^{-3}$  or  $T > 40 \text{ MeV}$ . In the spherical and adiabatic core collapse calculation of a massive star with the  $15M_\odot$  [47], the maximum density and temperature are found to be  $(\rho_B, T) = (0.24 \text{ fm}^{-3}, 22 \text{ MeV})$ , which do not reach the region of the above hyperon mixture region. It should be noted that this conclusion is model dependent. Hyperons may appear more abundantly in more realistic calculations with neutrino transfer, which are in progress.

We have also discussed the roles of pions in neutron stars and supernovae. In this work, we have examined the effects of free thermal pions [1]. In neutron star matter, the absolute value of the charge chemical potential  $\mu_C = \mu_p - \mu_n$  is calculated to be larger than the pion mass at  $\rho_B \gtrsim \rho_0$ , thus charged pions can condensate as far as the pion-nucleon interaction is not very repulsive. The EOS softening from pions is moderate and limited in the density range  $\rho_B < 0.88 \text{ fm}^{-3}$  without ( $p$ -wave)  $\pi N$  attraction, then the maximum mass of neutron stars ( $1.65M_\odot$ ) is almost the same as that without pions. In supernova explosions, temperatures are not very high and pion contributions are small. At higher temperatures as in the case of black hole formation or high energy heavy-ion collisions, the role of pions should be significant.

There are several points to be improved for deeper understanding of supernova matter EOS. First, it is necessary to examine the coupling constants of hyperons with hidden strangeness mesons,  $\zeta$  and  $\phi$ , which critically decide  $YY$  interaction. In this paper, we have adopted  $g_{\zeta Y}$  and  $g_{\phi Y}$  in Ref. [2], where the couplings are determined based on the SU(6) relation and a conjecture on the hyperon potential depth in hyperon matter. An alternative way to determine these couplings would be to invoke various hypernuclear and hyperon atom data, such as the double  $\Lambda$  hypernuclear binding energy in  ${}^6_{\Lambda\Lambda}\text{He}$  [49] and atomic energy shifts in  $\Sigma^-$  atom [34, 35, 36]. In Ref. [36], Tsubakihara et al. have determined the scalar couplings of  $g_{\sigma\Lambda}$ ,  $g_{\zeta\Lambda}$ ,  $g_{\sigma\Sigma}$  and  $g_{\zeta\Sigma}$ , by using the double  $\Lambda$  hypernuclear bond energy and the atomic energy shift of  $\Sigma^-$  atom, while vector couplings are fixed from the SU<sub>f</sub>(3) relations. At present, available data are so scarce that we cannot fix these couplings based on the data unambiguously, but future coming J-PARC and FAIR facilities will provide much more data on  $YY$  interaction. Next, it is desired to respect chiral symmetry in order to describe very dense matter, in which spontaneous broken chiral symmetry will be partially restored. A chiral symmetric RMF model [50] is recently developed based on a scalar meson self-energy derived in the strong coupling limit of lattice QCD, and it describes binding energies and radii of normal nuclei in a comparable precision to TM1. An SU<sub>f</sub>(3) extended version of this chiral RMF is now being developed [36]. Finally, distribution of finite nuclear species may be important at low densities [51]. At finite temperatures, the entropy increase by the formation of various fragments will contribute to gain the free energy compared

with the single heavy-nuclear configuration assumed in the Thomas-Fermi approach. It is not straightforward but challenging to include nuclear statistical equilibrium (NSE) distribution in a consistent way in the EOS based on RMF.

These challenging developments of hadronic and nuclear physics are important to understand the extreme conditions in compact objects and to clarify the mechanism of explosive phenomena in astrophysics.

## Acknowledgements

We would like to thank Dr. Daisuke Jido and Mr. Takayasu Sekihara for useful discussions. This work is supported in part by the Ministry of Education, Science, Sports and Culture, Grant-in-Aid for Scientific Research under the grant numbers, 15540243, 1707005, 18540291, 18540295 and 19540252, the 21st-Century COE Program "Holistic Research and Education Center for Physics of Self-organization Systems", and Yukawa International Program for Quark-hadron Sciences (YIPQS). The authors also would like to thank National Astronomical Observatory of Japan (NAOJ), Japan Atomic Energy Agency (JAEA), and Yukawa Institute for Theoretical Physics (YITP) for computing resources.

## Appendix A. Note on the EOS table

### Appendix A.1. Locations of data tables

The data tables are available on

`\protect\vrulewidth0pt`<http://nucl.sci.hokudai.ac.jp/~chikako/EOS/index.html>

or upon request to A. Ohnishi. On the web page, the tables under the name of '\*\*\*.tbl' (EOS table) and '\*\*\*.rat' (composition table) are available for the sets using  $U_{\Sigma}^{(N)} = -30, 0, +30, +90$  [MeV] at normal density. The most recommended potential is  $U_{\Sigma}^{(N)} = +30$  MeV. For other hyperons, we adopt the potential depth  $U_{\Lambda}^{(N)} = -30$  MeV and  $U_{\Xi}^{(N)} = -15$  MeV as described in section 2.1. The EOS table with thermal pions are available in addition to the standard choice without pions. As described in section 2.2, the set with thermal free pions are aimed only for the assessment of pion contributions in a simple treatment. Further careful treatment of pion interactions is necessary.

### Appendix A.2. Definition of quantities in the EOS table

We list the definitions of the physical quantities tabulated in the EOS table, '\*\*\*.tbl'. We note that the order of quantities in the list is partly different from the original Shen EOS table [16] since the current table contains lepton and photon contributions. The definitions of quantities follows the ones in Shen EOS unless stated specifically below.

- (1) Logarithm of baryon mass density:  $\log_{10}(\rho_B)$  [ $g/cm^3$ ]

The baryon mass density  $\rho_B$  is defined by

$$\rho_B = M_u n_B \tag{A.1}$$

where  $M_u$  and  $n_B$  are the atomic mass unit and the baryon number density, respectively.

- (2) Charge ratio:  $Y_C C = n_C/n_B$  The charge density  $n_C$  is defined by

$$n_C = \sum_B q_i n_i, \quad (\text{A.2})$$

where  $q_i$  and  $n_i$  are the charge and the number density of the baryons and the sum runs over the baryon octet.

- (3) Entropy per baryon:  $S/B$  [ $k_B$ ]

The entropy per baryon contains the contributions from hadrons, leptons and photons.

- (4) Temperature:  $T$  [MeV]

- (5) Pressure:  $P$  [MeV/fm<sup>3</sup>]

The pressure contains the contributions from hadrons, leptons and photons.

- (6) Chemical potential of neutron:  $\mu_n$  [MeV]

The chemical potential of neutron is measured relative to the nucleon mass  $M_N = 938$  MeV. It is connected with the baryon chemical potential as

$$\mu_n = \mu_B - M_N \quad (\text{A.3})$$

- (7) Chemical potential of proton:  $\mu_p$  [MeV]

The chemical potential of proton is measured relative to the nucleon mass  $M_N$ . The relation to the baryon and charge chemical potentials reads

$$\mu_p = \mu_B + \mu_C - M_N \quad (\text{A.4})$$

- (8) Chemical potential of electron:  $\mu_e$  [MeV]

The chemical potential of electron is determined by the charge neutrality as

$$n_e = \sum_B q_i n_i. \quad (\text{A.5})$$

See below for the descriptions on the lepton contributions.

- (9) Free neutron fraction:  $Y_n$

In the uniform matter, the free neutron fraction is simply the ratio,  $n_n/n_B$ . For the non-uniform matter at low density, the definition follows the one in Shen EOS.

- (10) Free proton fraction:  $Y_p$

The ratio,  $n_p/n_B$ , as in  $Y_n$  above. For the fraction of strangeness baryons, see the description below on the table of number fractions.

- (11) Mass number of heavy nucleus:  $A$

The values of from (11) to (14) are taken from Shen EOS table or zero set above normal nuclear density.

- (12) Charge number of heavy nucleus:  $Z$

- (13) Heavy nucleus fraction:  $X_A$



- (14) Alpha-particle fraction:  $X_\alpha$
- (15) Energy per baryon:  $E/B$  [MeV]  
The energy per baryon is defined with respect to the free nucleon mass  $M_N$  and contains the contributions from hadrons, leptons and photons.
- (16) Free energy per baryon:  $F/B$  [MeV]  
The free energy per baryon is defined with respect to the atomic mass unit  $M_u$  and contains the contributions from hadrons, leptons and photons.
- (17) Effective mass:  $M^*$  [MeV]  
The effective mass of nucleon is obtained in the RMF theory for uniform matter. In non-uniform matter, we replace the effective mass  $M_N^*$  by the free nucleon mass  $M_N$ .

### Appendix A.3. Data table of composition

In order to provide the information on the appearance of hyperons other than nucleons, we prepare a separate data table (\*\*\*.rat) for the number fractions. The number fraction,  $Y_i = n_i/n_B$ , is given as a function of  $(\rho_B, T, Y_C)$  in the following order.

- (1) Logarithm of baryon mass density:  $\log_{10} \rho_B$  [g/cm<sup>3</sup>]
- (2) Temperature:  $T$  [MeV]
- (3) Charge ratio:  $Y_C$
- (4) Neutron ratio (including neutrons in alpha):  $Y_n$
- (5) Proton ratio (including protons in alpha):  $Y_p$
- (6)  $\Lambda$  ratio:  $Y_\Lambda$
- (7)  $\Sigma^-$  ratio:  $Y_{\Sigma^-}$
- (8)  $\Sigma^0$  ratio:  $Y_{\Sigma^0}$
- (9)  $\Sigma^+$  ratio:  $Y_{\Sigma^+}$
- (10)  $\Xi^-$  ratio:  $Y_{\Xi^-}$
- (11)  $\Xi^0$  ratio:  $Y_{\Xi^0}$

### Appendix A.4. Treatment of leptons

We describe briefly on the contribution of leptons (electrons, muons and neutrinos) in the current study.

We remark that we take into account muons in the case of cold neutron stars. Muons appear abundantly at densities higher than the threshold when the electron chemical potential exceeds the muon rest mass. The chemical potentials of electrons and muons are related with

$$\mu_\mu = \mu_e \tag{A.6}$$

This is because neutrinos freely escape from the neutron star and are not trapped inside. Accordingly, the contributions of electrons and muons are taken into account in the discussions of cold neutron stars.

For the EOS table for core-collapse supernovae, we add the contributions of electrons, positrons and photons while muons are not added because of the following reason. In the supernova cores, neutrinos are trapped inside the supernova core and the Fermi energies of neutrinos becomes high and non-zero. If the chemical equilibrium holds, the chemical potentials follows the relations,

$$\mu_\mu - \mu_{\nu_\mu} = \mu_e - \mu_{\nu_e} , \quad (\text{A.7})$$

$$n_\mu + n_{\nu_\mu} = 0 . \quad (\text{A.8})$$

The latter relation comes from the fact that the net  $\mu$ -type lepton number is zero. Because of positive values of  $\mu_{\nu_e}$ , r.h.s of the chemical equilibrium is reduced. In addition, the appearance of muon requires the production of anti-neutrinos of  $\mu$ -type and leads to the negative value of  $\mu_{\nu_\mu}$ . Therefore, the appearance of muons are suppressed in supernova core.

Contributions of neutrinos are not added because the treatment depends on the density region. In the central part of supernova core, neutrinos are trapped and the chemical equilibrium are reached together with neutrinos. Outside the neutrino trapping surface, typically at  $\sim 10^{11}$  g/cm<sup>3</sup>, neutrinos escape freely and neutrinos do not contribute. They also depend on the method of neutrino-radiation in numerical simulations.

## References

- [1] Glendenning N K 2000 "Compact Stars: Nuclear Physics, Particle Physics and General Relativity" (Springer-Verlag, Berlin, 2000), and references therein.
- [2] Schaffner J and Mishustin I 1996 *Phys. Rev. C* **53** 1416
- [3] Balberg S and Gal A 1997 *Nucl. Phys. A* **625** 435
- [4] Sahu P K and Ohnishi A 2001 *Nucl. Phys. A* **691** 439c
- [5] Nishizaki S, Takatsuka T and Yamamoto Y 2002 *Prog. Theor. Phys.* **108** 703; Baldo M, Burgio G F and Schulze H J 2000 *Phys. Rev. C* **61** 055801; Vidana I, Polls A, Ramos A, Hjorth-Jensen M and Stoks V G J 2000 *Phys. Rev. C* **61** 025802;
- [6] Sugahara Y and Toki H 1994 *Prog. Theor. Phys.* **92** 803
- [7] Shen H 2002 *Phys. Rev. C* **65** 035802
- [8] Kunihiro T, Takatsuka T, Tamagaki R and Tatsumi T 1993 *Prog. Theor. Phys. Suppl.* **112** 123, and references therein.
- [9] Kaplan D B and Nelson A E 1986 *Phys. Lett. B* **175** 57; Lee C H 1996 *Phys. Rep.* **275** 255; Weber F 2005, *Prog. Part. Nucl. Phys.* **54** 193; Bailin D and Love A 1984 *Phys. Rept.* **107** 325; Alford M G, Rajagopal K and Wilczek F 1999 *Nucl. Phys. B* **537** 443
- [10] Sumiyoshi K, Suzuki H, Yamada S and Toki H 2004 *Nucl. Phys. A* **730** 227
- [11] Sumiyoshi K, Yamada S, Suzuki H, Shen H, Chiba S and Toki H 2005 *Astrophys. J.* **629** 922.
- [12] Sumiyoshi K, Yamada S, Suzuki H, Chiba S 2006 *Phys. Rev. Lett.* **97** 091101
- [13] Sumiyoshi K, Yamada S, Suzuki H 2007 *Astrophys. J.* **667** 382
- [14] For recent progresses, see, for example, Gyulassy M and McLerran L 2005 *Nucl. Phys. A* **750** 30
- [15] Lattimer J M and Swesty F D 1991 *Nucl. Phys. A* **535** 331

- [16] Shen H, Toki H, Oyamatsu K and Sumiyoshi K 1998 *Prog. Theor. Phys.* **100** 1013
- [17] Sugahara Y and Toki H 1994 *Nucl. Phys. A* **579** 557
- [18] Suzuki H 1994 "Physics and Astrophysics of Neutrinos", edited by M. Fukugita and A. Suzuki (Springer-Verlag, Berlin), 763
- [19] Pons J A, Reddy S, Prakash M, Lattimer J M, Miralles J A 1999 *Astrophys. J* **513** 780;  
Pons J A, Miralles J A, Prakash M, and Lattimer J M 2001 *Astrophys. J* **553** 382
- [20] Noumi H *et al* 2002 *Phys. Rev. Lett.* **89** 072301 [Erratum: *Phys. Rev. Lett.* **90** (2003) 049902];  
Saha P K *et al* 2004 *Phys. Rev. C* **70** 044613
- [21] Harada T and Hirabayashi Y 2006 *Nucl. Phys. A* **759** 143; *Nucl. Phys. A* **767** 206
- [22] Kohno M *et al* 2004 *Prog. Theor. Phys.* **112** 895; Kohno M, Fujiwara Y, Watanabe Y, Ogata K  
and Kawai M 2006 *Phys. Rev. C* **74** 064613
- [23] Maekawa H 2008 *PhD Thesis* Hokkaido University; Maekawa H, Tsubakihara K, Matsumiya H  
and Ohnishi A 2008 in preparation
- [24] Aoki S *et al.* 1995 *Phys. Lett. B* **355** p 45
- [25] Fukuda T *et al.* 1998 *Phys. Rev. C* **58** p 1306; Khaustov P *et al.* 2000 *Phys. Rev. C* **61** p 054603
- [26] Maekawa H, Tsubakihara and Ohnishi A 2007 *Euro. Phys. J. A* **33** 269 (*Preprint* nucl-th/0701066)
- [27] Maekawa H, Tsubakihara K, Matsumiya H and Ohnishi A 2007 (*Preprint* arXiv:0704.3929 [nucl-th])
- [28] Danielewicz P, Lacey R and Lynch W G 2002 *Science* **298** 1592
- [29] Sahu P K, Cassing W, Mosel U and Ohnishi A 2000 *Nucl. Phys. A* **672** 376
- [30] Isse M, Ohnishi A, Otuka N, Sahu P K and Nara Y 2005 *Phys. Rev. C* **72** 064908
- [31] Niksic T, Vretenar D and Ring P 2002 *Phys. Rev. C* **66** 064302
- [32] Brockmann R and Machleidt R 1990 *Phys. Rev. C* **42** 1965
- [33] Nagae T *et al* 1998 *Phys. Rev. Lett.* **80** 1605; Harada T, Shinmura S, Akaishi Y and Tanaka H  
1990 *Nucl. Phys. A* **507** 715; Harada T 1998 *Phys. Rev. Lett.* **81** 5287
- [34] Batty C J, Friedman E and Gal A 1994 *Phys. Lett. B* **335** 273; *Prog. Theor. Phys. Suppl.* **117** 227
- [35] Mares J, Friedman E, Gal A and Jennings B K 1995 *Nucl. Phys. A* **594** 311
- [36] Tsubakihara K, Maekawa H, Ohnishi A 2007 *Euro. Phys. J. A* **33** 295 (*Preprint* nucl-th/0702008)
- [37] Kohno M *et al* 2000 *Nucl. Phys. A* **674** 229
- [38] Rikovska-Stone J, Guichon P A M , Matevosyan H H and Thomas A W 2007 *Nucl. Phys. A* **792**  
341
- [39] Kaiser N 2005 *Phys. Rev. C* **71** 068201
- [40] Knorren R, Prakash M and Ellis P J 1995 *Phys. Rev. C* **52** 3470
- [41] Menezes D P and Providencia C 2003 *Phys. Rev. C* **68** 035804
- [42] Sumiyoshi K, Ishizuka C, Ohnishi A, Yamada S, Suzuki H 2008, in preparation.
- [43] Suzuki K *et al.* 2004 *Phys. Rev. Lett.* **92** 072302; Hirenzaki S, Toki H and Yamazaki T 1991 *Phys. Rev. C* **44** 2472; Itahashi K *et al.* 2000 *Phys. Rev. C* **62** 025202
- [44] Batty C J, Friedman E and Gal A 1983 *Nucl. Phys. A* **402** 411
- [45] Kienle P and Yamazaki T 2004 *Prog. Part. Nucl. Phys.* **52** 85
- [46] Friedman E *et al.* 2004 *Phys. Rev. Lett.* **93** 122302
- [47] Woosley S E and Weaver T A 1995 *Astrophys. J. Suppl.* **101** 181
- [48] Thorsson V, Prakash M and Lattimer J M 1994 *Nucl. Phys. A* **572** 693 (Erratum-ibid. A **574** 851)  
Keil W and Janka H T 1995 *Astron. Astrophys.* **296** 145 Prakash M, Cooke J R and Lattimer J M  
1995 *Phys. Rev. D* **52** 661 Prakash M, Bombaci I, Prakash M, Ellis P J, Lattimer J M and  
Knorren R 1997 *Phys. Rept.* **280** 1 Vidana I, Bombaci I, Polls A and Ramos A 2003 *Astron. Astrophys.* **399** 687
- [49] Takahashi H *et al* 2001 *Phys. Rev. Lett.* **87** 212502
- [50] Tsubakihara K and Ohnishi A 2007 *Prog. Theor. Phys.* **117** 903 (*Preprint* nucl-th/0607046)
- [51] Ishizuka C, Ohnishi A and Sumiyoshi K 2003 *Nucl. Phys. A* **723** 517